Modeling Potassium Capture by Aluminosilicate, Part 1: Kaolin

Hashemi, Hamid; Wang, Guoliang; Jensen, Peter Arendt; Wu, Hao; Frandsen, Flemming Jappe; Sander, Bo; Glarborg, Peter

Published in:
Energy and Fuels

Link to article, DOI:
10.1021/acs.energyfuels.1c01382

Publication date:
2021

Document Version
Peer reviewed version

Modelling Potassium Capture by Aluminosilicate, Part 1: Kaolin

Hamid Hashemi,*,† Guoliang Wang,† Peter Arendt Jensen,† Hao Wu,† Flemming Jappe Frandsen,† Bo Sander,‡ and Peter Glarborg†

†*DTU Chemical Engineering, Technical University of Denmark, DK-2800 Lyngby, Denmark*

‡*Ørsted Bioenergy & Thermal Power A/S, Kraftværksvej 53, 7000 Fredericia, Denmark*

E-mail: hah@kt.dtu.dk

Abstract

Additives rich in Si and Al such as kaolin may be applied in PF biomass boilers to fix alkali metals in species that are more benign than the alkali salts released in biomass combustion. In this study, models for the reaction of gas-phase potassium salts with kaolin particles is developed for the conditions appearing in PF boilers such as short residence times, high temperatures, and small size of the additive particles. The reaction between gaseous potassium components and kaolin particles has been modelled with a Shrinking Core Model (SCM) and a Uniform Conversion Model (UCM). The SCM model takes into account the effects of chemical kinetics, diffusion in a gas film surrounding the particle, diffusion in a product layer, and thermochemical equilibrium on the reaction progress. The UCM model covers diffusion in a gas film surrounding the particle, chemical kinetics, and thermochemical equilibrium. Both models are able to accommodate the effects of change in temperature, particle size, reaction time, and potassium component concentration. Literature data from experiments in an entrained flow-reactor (EFR) at 800–900° C were used to derive the chemical kinetic rate coefficients of the reaction between kaolin and KOH. The models then were evaluated against

experimental data for alkali salts of KCl, KOH, K_2CO_3 and K_2SO_4 covering temperatures of 800–1450° C, kaolin particle sizes of 4–14 μm, residence time of 0.8–1.9 s, and salt to additive molar ratios of 0.05–0.96. The evaluation indicated that both SCM and UCM were suitable for a wide range of conditions, but the UCM captured better the effect of particle size. The modelling outcomes suggested that if reaction time was long enough, the thermochemical equilibrium would be the major limitation in capturing potassium by kaolin at high temperatures and high potassium concentrations. At lower temperatures, however the conversion was mainly limited by chemical kinetics. The mass-transfer limitation was less critical under the investigated conditions. The developed models can account for the reaction of gas phase potassium salts with kaolin at local conditions relevant to PF boilers using biomass.

Introduction

Biomass is widely used for producing heat and electricity in existing power plants designed for coal combustion, e.g., in pulverized-fuel (PF) combustion boilers. Reaction temperature in PF boilers might be as high as 1800° C and the residence time in the hot zone is very short, demanding very fine fuel particles to achieve complete conversion. A challenge in burning biomass in PF boilers is its content of alkali metals. Higher alkali contents might lead to increased ash deposition[1] and aerosol formation[2]. Gaseous alkali salts from biomass combustion are transferred with the flue gas and deposited on boiler surfaces, accelerating corrosion[3] and deactivation of SCR catalyst[4–6]. Using fuel additives is a promising technique to solve this problem in PF boilers[7]. The additives react with gas-phase alkali salts and form components with higher melting temperature and less corrosivity.

Additives investigated for capturing alkali salt can be categorized based on their major elements as Al/Si-based, S-based, P-based, and Ca-based[7]. Among the Al/Si-based additives, kaolin and coal fly-ash (CFA) have been investigated extensively [7–51]. Earlier studies of alkali capture by aluminosilicate additives have focused on capturing potassium[7–13,19,20] and

sodium[14–18,20–28,49]. Tran et al.[12] studied potassium capture by kaolin in a fixed-bed reactor for additive particles of 0.5–2 mm at 750–950° C while the gas residence time in the bed has been 4–11 ms. They suggested that the process was mainly controlled by chemical kinetic under their conditions. Zheng et al.[13] measured the potassium capture by kaolin and CFA pellets with a diameter of 1.6 mm in a fixed-bed reactor at 900–1500° C. They found that the diffusion of potassium salt controlled the reaction to a large extent under the investigated conditions. The additive pellets in ref[11–13] were exposed to reaction temperature for several hours, which promotes the effects of phase transformation, melting, and sintering on the reaction progress, while residence time of additives suspended in PF boilers is very short; in an order of a few seconds.

The most relevant studies to conditions in PF boilers have been conducted by Gale et al.[17] and Wang et al.[7–10]. Gale et al. studied the reaction between kaolin aerosol and gaseous sodium at temperatures below 1230° C and suggested that the sodium capture is mainly controlled by chemical kinetic. Wang et al. investigated potassium capture by kaolin[7,8] and coal fly-ash[9,10] using an entrained flow reactor at 800–1450° C. They found that equilibrium has a large influence on the conversion at higher temperatures, and the efficiency of kaolin in capturing potassium is a function of both the system inlet composition and the operational conditions, i.e., temperature, gas residence time, salt to additive ratio, and particle size. Since the amount and type of salts varies for different biomasses, predictive tools are beneficial for power plant operators/designers to adjust additive amount and particle size accordingly.

Modelling alkali capture by kaolin and coal fly-ash needs incorporating the chemical kinetics of the reaction between alkali and additive, the diffusion of alkali salt into additive particles, and the chemical equilibrium limitations[7,8]. Earlier models for alkali reactions with aluminosilicate additives [12–18] have been evaluated at temperatures lower than those found in PF boilers, and all except ref[17] have been developed using experimental data from large particles, which complicates extracting kinetic information due to significant potassium gradients inside the particles. Very recently, Zhu et al.[49] suggested a model for potassium

capture by kaolin under the conditions of PF boilers. They relied heavily on EFR data from Wang et al.[7,8] for both chemical kinetic and additive deactivation.

The aim of this work is to develop a model to predict the conversion of gaseous potassium compounds to thermally stable products in potassium reaction with kaolin particles under conditions of PF boilers, i.e., temperatures of 800–1700° C and short residence times. Two chemical engineering approaches for modelling gas-solid interaction, the Shrinking Core Model (SCM) and the Uniform Conversion Model (UCM), are investigated. The models are evaluated against extensive entrained flow-reactor measurements provided in ref[7,8] which covered a wide range of temperature (800–1450° C), reaction time (0.8–1.9 s), kaolin particle size (3.5–13.5 μm), and potassium-to-kaolin molar ratio (0.05–0.96) in the feed mixture.

Model

Two modelling approaches, SCM and UCM are investigated for the reaction between solid kaolin particles and gaseous potassium compounds. The SCM and UCM have been used for modelling gas-solid reactions for a wide range of applications[52]. Due to small particles investigated here, temperature gradient inside the particle has been neglected. A brief overview of SCM and UCM is given here, and further details can be found in the supporting information.

Uniform Conversion Model (UCM)

In the Uniform Conversion Model (UCM), it is assumed that reaction occurs continuously throughout the particle[52] and the concentration of gaseous alkali salt is constant within the particle. The particle size remains constant, independent of the degree of conversion. Outside the particle, the alkali concentration varies with location only inside a film surrounding the solid particle. This model is a good approximation when mass transfer inside the particle is fast enough and does not inhibit additive conversion.

The stoichiometric reaction between kaolin and alkali salt is assumed as R1.

$$\text{Kaolin (s)} + \Psi\ \text{K (g)} \xrightarrow{\text{k}_{\text{c, UCM}}} \text{Products (s)} \tag{R1}$$

The stoichiometric coefficient is shown by Ψ. The rate of reaction R1 is assumed to be first order in K and kaolin concentrations, and is given by equation (1).

$$RR_{UCM} = -k_{c,UCM} \times [Kaolin] \times [K] \tag{1}$$

Here, $\text{k}_{c,UCM}$ is the reaction rate coefficient, $[Kaolin]$ is the concentration of kaolin in a single particle, and $[K]$ is the concentration of potassium (from salt) inside the kaolin particle. After establishing transport and kinetic equations (see supporting information for details), the final model can be represented by a set of ordinary differential equations given in equations (2) and (3).

$$\frac{dN_{kaolin}}{dt} = -\frac{4\pi}{\Psi} \times k_{overall,\,UCM} \times [K]_\infty \tag{2}$$

$$\frac{d[K]_\infty}{dt} = \Psi\ \beta\ \frac{dN_{kaolin}}{dt} \tag{3}$$

Here, t is time, N_{kaolin} is the mole number of unreacted kaolin in an individual particle, $[K]_\infty$ is the free-stream concentration of potassium (as K atoms), β is the number of kaolin particles per gas volume, and $k_{overall,\,UCM}$ is the overall rate coefficient given by equation 4.

$$\frac{1}{k_{overall,\,UCM}} = \frac{1}{k_g\, r_i^2} + \frac{4\pi}{\Psi\ k_{c,UCM}\ N_{kaolin}} \tag{4}$$

The mass transfer coefficient of the potassium salt in the gas phase is shown by k_g, and the initial radius of the kaolin particle is represented by r_i.

Shrinking Core Model (SCM)

In the SCM approach, it is assumed that the reaction only occurs at the outer surface of an unreacted core. As the reaction progresses, the reactive surface moves into the particle and leaves behind a layer of products[52], so the unreacted core shrinks. The model accounts for diffusion through the product layer (product-layer diffusion), diffusion through the gas-film outside the particle (external diffusion), and chemical kinetic. Similar to UCM, the stoichiometric reaction is represented by reaction R1.

$$\text{Kaolin (s)} + \Psi\ \text{K (g)} \xrightarrow{\text{k}_{\text{c,SCM}}} \text{Products (s)} \tag{R1}$$

The reaction rate (RR_{SCM}) is calculated by equation (5).

$$RR_{SCM} = -k_{c,SCM} \times A \times [K] \tag{5}$$

Here, $k_{c,SCM}$ denotes the reaction rate coefficient and A represents the surface area of the unreacted core. The final model (see supporting information) can be represented by an ODE set given in equations (6) and (7).

$$\frac{dr_s}{dt} = -\frac{1}{\Psi} \times \frac{MW_{kaolin}}{\rho_{kaolin}} \times k_{overall,SCM} \times [K]_\infty \tag{6}$$

$$\frac{d[K]_\infty}{dt} = -4\,\pi r_s^2 \beta \times k_{overall,SCM} \times [K]_\infty \tag{7}$$

Here, MW_{kaolin} is the molar mass of kaolin, ρ_{kaolin} is the density of kaolin, and r_s is the radius of the unreacted core. The overall rate coefficient ($\text{k}_{overall,SCM}$) is given by equation (8).

$$\frac{1}{k_{overall,SCM}} = \frac{r_s^2}{r_i^2\ k_g} + \frac{r_s}{D_{eff}}\left(1 - \frac{r_s}{r_i}\right) + \frac{1}{\Psi\ k_{c,SCM}} \tag{8}$$

D_{eff} represents the effective diffusion coefficient of potassium salt in the product layer. The separate terms in equation (8) represent different resistances controlling the overall conver-

sion; $\frac{r_s^2}{r_i^2\, k_g}$ is the external diffusion resistance, $\frac{r_s}{D_{eff}}\left(1-\frac{r_s}{r_i}\right)$ is the product-layer diffusion resistance, and $\frac{1}{\Psi\, k_{c,SCM}}$ is the kinetic resistance.

The external gas-phase mass transfer coefficient (k_g) can be found via equation (9).

$$k_g = \frac{1}{2r_i} \times Sh \times D_{Salt} \tag{9}$$

Here, Sh is the Sherwood number which can be related to the Reynolds (Re) and Schmidt (Sc) numbers using the Froessling equation (10).

$$Sh = 2 + 0.552 \times Re^{\frac{1}{2}}\, Sc^{\frac{1}{3}} \tag{10}$$

For small particles in the Stokes regime, the second term on the right side of equation (10) is negligible, so $Sh \simeq 2 \longrightarrow k_g \simeq \frac{D_{Salt}}{r_i}$.

The binary diffusion coefficient of the salt in the gas-phase (D_{Salt}) can be approximated by the diffusion coefficient in neat nitrogen. Here, $D_{Salt,\,N_2}$ is estimated following ref[53] using Lennard-Jones parameters from ref[54,55]. Temperature sensitivity of D_{Salt} is estimated by equation (11).

$$D_{Salt} \simeq D_{Salt,\,0}\ \times\ \left(\frac{T}{T_0}\right)^{1.75} \tag{11}$$

$D_{Salt,\,0}$ is the diffusion coefficient at reference conditions (T_0 = 298 K, P_0 = 1 atm). For porous materials, D_{eff} can be approximated[56] by equation (12).

$$D_{eff} = \frac{D_{Salt} \cdot \phi_p \cdot \sigma_c}{\Gamma} \tag{12}$$

where ϕ_p is porosity, Γ is tortuosity, and σ_c is the constriction factor of the particle.

Properties of Kaolin and Potassium Salts

The elemental composition of the investigated samples of kaolin in ref[7,8] is given in Table 1. The physical and chemical properties of kaolin can vary significantly, depending on the source and preparation procedure. Reported density of kaolin varies between 1300 and 2650 ($kg\ m^{-3}$)[12,18,57]. Here, a density of 2650 ($kg\ m^{-3}$) proposed by Kerscher et al.[18] is adopted. Tortuosity, porosity, and constriction factor of kaolin particles are estimated (see Table 2).

Table 1: Elemental composition (dry) of kaolin in experiments by Wang et al.[7,8].

Element	Normal & Fine Kaolin ($D_{50,\,add.} = 5.5$ & $3.5\,\mu m$)		Coarse Kaolin ($D_{50,\,add.} = 13.5\,\mu m$)	
	mass ratio [%]	molar ratio [%]	mass ratio [%]	molar ratio [%]
O	56.9	69.75	55.88	68.88
Si	22	15.36	23	16.15
Al	19	13.81	19	13.89
K	1.1	0.55	1.2	0.61
Fe	0.47	0.17	0.46	0.16
Ca	0.1	0.05	0.1	0.05
Mg	0.14	0.11	0.12	0.10
Na	0.1	0.09	0.1	0.09
P	0.05	0.03	0.05	0.03
Cl	0.1	0.06	0.05	0.03
S	0.02	0.01	0.03	0.02

Table 2: Properties of investigated kaolin and potassium salts.

Properties	Value/Unit	Ref./Note
Density of raw kaolin	2650 kg/m^3	see text,[18]
Kaolin tortuosity (Γ)	3	est.[a]
Kaolin porosity (ϕ_p)	0.5	est.[a]
Kaolin constriction factor (σ_c)	0.8	est.[a]
$D_{0,\,\mathrm{KOH\ in\ N_2}}$	8.6×10^{-6} m^2/s	calculated [b]

$D_{0,\,\mathrm{KCl\ in\ N_2}}$	7.9×10^{-6} m^2/s	calculated [b]
MW_{Kaolin}	10 kg /mol	assumed [c]

[a] Similar pore properties are assumed for both raw kaolin and reacted kaolin.

[b] Calculated at 298 K and 1 atm. See supporting information for details.

[c] One mole of kaolin is assumed equal to 10 kg of kaolin, i.e., the Kaolin is assumed to be a pseudo-molecule with formula of $O_{356}\,Si_{78}\,Al_{70}\,K_3\,Fe\,Mg$.

Chemical Reaction and Equilibrium Constraint

A one-step global reaction (R1) is considered in both modelling approaches, while in reality the reaction is much more complicated and consists of several competing steps. If kaolin heats up in the absence of any alkali components, it decomposes to metakaolin and water at ∼450 ℃[58], according to reaction R2.

$$(SiO_2)_2\,.\,(Al_2O_3)\,.\,(H_2O)_2\,(\text{kaolinite}) \longrightarrow (SiO_2)_2\,.\,(Al_2O_3)\,(\text{metakaolin}) + 2\,H_2O \qquad \text{(R2)}$$

Above ∼980 ℃ and after a sufficiently long reaction time, metakaolin transforms to a spinel and an amorphous structure following reaction R3.

$$(SiO_2)_2\,.\,(Al_2O_3)\,(\text{metakaolin}) \longrightarrow SiAl_2O_4\,(\text{spinel}) + SiO_2\,(\text{amorphous}) + \frac{1}{2}\,O_2 \qquad \text{(R3)}$$

As the temperature approaches ∼1100 ℃, mullite might be formed gradually via reaction R4.

$$3\,SiAl_2O_4\,(\text{spinel}) + 3\,SiO_2\,(\text{amorphous}) + \frac{3}{2}\,O_2 \longrightarrow$$
$$(Al_2O_3)_3 \cdot (SiO_2)_2\,(\text{mullite}) + 4\,SiO_2\,(\text{amorphous}) \qquad \text{(R4)}$$

The aforementioned transformation of kaolin affects its reactivity considerably. Among

the different products of kaolinite calcination, metakaolin is expected to be the most efficient agent in capturing alkali salts while mullite is the least effective one[7]. The reactions between metakaolin and KOH can take place via reactions R5 and R6[7,59].

$$Al_2O_3(SiO_2)_2\,(\text{metakaolin}) + 2\,KOH \longrightarrow 2\,KAlSiO_4\,(\text{kalsilite}) + H_2O \qquad \text{(R5)}$$

$$Al_2O_3(SiO_2)_2\,(\text{metakaolin}) + 2\,KOH + 2\,SiO_2 \longrightarrow 2\,KAlSi_2O_6\,(\text{leucite}) + H_2O \qquad \text{(R6)}$$

In addition to kaolinite transformation, the thermochemical equilibrium plays a critical role for kaolin reactions by limiting the formation of some products and favouring the formation of others, especially at higher temperatures[7]. As the products of the stoichiometric reaction vary with conditions, the stoichiometric coefficient (Ψ) adapts accordingly, which introduces further complexity in modelling.

To facilitate modelling the effects of phase-change and equilibrium constraints on potassium capture, a two-step scheme is implemented here. In the first step (R1a), it is assumed that the reaction proceeds irreversibly to give a pseudo component called *Products**.

$$\text{Kaolin} + \Psi\ \text{Salt} \xrightarrow{k_{overall}} \text{Products}^* \qquad \text{(R1a)}$$

This step is controlled by kinetic and diffusion resistances, and a constant nominal stoichiometry (Ψ) is assumed for all conditions. In the second step (R1b), it is assumed that *Products** dissociate immediately to give the final products.

$$\text{Products}^* \xrightarrow{\text{fast}} (\Omega)\ \ K_{Captured} + (1\text{-}\Omega)\,K_{non-Captured} + \text{Other components} \qquad \text{(R1b)}$$

Here, Ω is an equilibrium ceiling defined as the ratio of captured-K to the total-K at equilibrium stage and varies between zero and unity. The value of Ω is quantified from the results

of equilibrium calculations, and the salt conversion from R1a will be corrected according to equation (13).

$$X_{K,\,corrected} = X_{K,\,R1a} \times \Omega \tag{13}$$

This engineering approximation allows tabulation of equilibrium data in the form of equilibrium ceiling (Ω), which makes storing and recalling the data much easier in the solution algorithm.

Any Al or Si atom in the kaolin can be counted as an active atom if a similar reactivity with potassium is assumed for both Al and Si. In reactions R5 (and R6), 4 (and 6) active atoms are needed to capture two atoms of K. For simplicity, it is assumed that in a stoichiometric reaction, each potassium atom always needs two active atoms. Therefore, Ψ can be assumed equal to the half of total active atoms in the kaolin. Later, it will be shown that at intermediate temperatures, full conversion of potassium is possible when the feed molar ratio of $\frac{K}{Al+Si}$ is 0.5, so assuming Ψ equal to $0.5 \times (Al + Si)$ is not unreasonable. In an earlier model developed for sodium capturing with kaolin[17], it was assumed that each Na atom needs one Al atom for the stoichiometric reaction. As molar fractions of Al and Si in kaolin is close, our assumption is in line with those made in ref[17].

Kaolin in reaction R1 is a pseudo species defined according to elemental distribution in the kaolin sample. Here, one mole of *Kaolin* is defined as 10 kg of raw kaolin, i.e., *Kaolin* = $O_{356}\,Si_{78}\,Al_{70}\,K_3\,Fe\,Mg$. Then, Ψ will be 74.

The equilibrium module of *FactSage 7.3*[60] is used to calculate Ω. The databases of *FactPS*, *FToxid*, *FTsalt*, and *FTpulp* are employed for the calculations. Only ideal gas, pure liquids, and pure solids are selected as possible phases of products, following Wang et al.[7]. Under the conditions of the study, leucite ($KAlSi_2O_6$), sanidine ($KAlSi_3O_8$), and kaliophilite ($KAlSiO_4$) are the most common products when potassium is captured by kaolin. Other common K-components are listed in Table 3. The equilibrium ceiling of potassium capture (Ω) will be shown alongside the experimental data and the model predictions for all investigated series.

Table 3: Major K-components encountered in present equilibrium calculations.

	Components				
non-captured K:	KOH	KCl	K	KO	K_2SO_4
captured K:	$KAlSi_2O_6$	$KAlSi_3O_8$	$KAlSiO_4$	K_2SiO_3	$KAlO_2$
	$K_2Si_2O_5$	$K_{10}Mg_5Si_{11}O_{32}$	$K_2MgSi_3O_8$	$K_2MgSi_3O_8$	

Results and Discussion

The results of experiments with mixtures of potassium salts and kaolin fed to an entrained flow reactor (EFR)[7,8] are used to parameterize and evaluate the models. An overview of the data is given in Table 4 and further details can be found in the references[7,8]. In the experiments, the reactions of KOH, KCl, K_2CO_3 and K_2SO_4 with kaolin were investigated. The salts and kaolin were injected as a liquid slurry into the reactor. After quick evaporation of the salts, they reacted with kaolin particles in the hot zone of the reactor. The products were then quenched at the reactor exit and the solid residuals were analysed to quantify the potassium capture. Effects of temperature (800–1450° C), salt concentration (50–1000 ppm), reaction time (0.8–1.9 s), and particle size of kaolin (3.5–13.5 μm) were explored. In the experiments, the variations of salt concentration is much wider than those found in industrial PF boilers. Potassium carbonate (K_2CO_3) dissociates immediately at the temperatures of this study[8]. Products of dissociation in the presence of water are expected to be KOH and CO_2. Consequently, tests with K_2CO_3 are used to confirm the KOH experiments.

Here, the particle residence time is approximated by the gas residence time. The conversion of the potassium salts in the absence of kaolin in a mixture containing 5% water and 20% oxygen (typical of the EFR experiments) was investigated with *Chemkin*[61] and a gas-phase chemical kinetic model developed in ref.[62] Results (supporting information) indicate that the conversion of KCl to KOH increases with temperature, and will be 1–13% at temperatures of 800–1450° C. The conversion is quite fast, so the reaction reaches equilibrium in less than 1.0 ms. Equilibrium simulations using *FactSage* confirm maximum 13% KCl conversion to KOH at 1450° C.

Table 4: Overview of kaolin + potassium salts experiments. Experimental data of kaolin + KOH are from ref[7], and for kaolin reactions with other salts are from ref[8].

Exp. No.	T [C]	τ [s] [a]	$D_{50,\,add.}$ [μ m] [b]	K Conc. [ppm] [c]	$\left(\frac{K}{Al+Si}\right)$ [molar] [d]	$X_{K,\,exp}$ [mol %] [e]	$X_{K,\,equi}$ [mol %] [f]	$X_{(Al+Si)}$ [mol %] [g]
				Kaolin + KOH				
KOH-A	1100	1.2	5.5	50	0.05	96	100	9
	1100	1.2	5.5	250	0.24	95	100	46
	1100	1.2	5.5	500	0.48	85	95	82
	1100	1.2	5.5	750	0.72	54	71	78
	1100	1.2	5.5	1000	0.96	40	54	77
KOH-A*	1100	1.2	5.5	50	0.05	84	100	8
(K_2CO_3)	1100	1.2	5.5	500	0.48	81	95	78
	1100	1.2	5.5	1000	0.96	41	54	78
KOH-B	800	1.2	5.5	50	0.05	88	100	8
	900	1.2	5.5	50	0.05	92	100	9
	1100	1.2	5.5	50	0.05	96	100	9
	1300	1.2	5.5	50	0.05	96	100	9
	1450	1.2	5.5	50	0.05	96	99	9
KOH-C	800	1.2	5.5	500	0.48	62	99	60
	900	1.2	5.5	500	0.48	72	98	69
	1100 [h]	1.2	5.5	500	0.48	85	95	82
	1300	1.2	5.5	500	0.48	88	91	85
	1450	1.2	5.5	500	0.48	74	73	71
KOH-C*	800	1.2	5.5	500	0.48	59	99	57
(K_2CO_3)	900	1.2	5.5	500	0.48	75	98	72
	1100	1.2	5.5	500	0.48	81	95	78
	1300	1.2	5.5	500	0.48	86	91	83
	1450	1.2	5.5	500	0.48	76	73	73
KOH-D	800 [i]	1.2	5.5	500	0.48	62	99	60
	800	1.5	5.5	500	0.48	70	99	67
	800	1.9	5.5	500	0.48	78	99	75
KOH-E	1100	1.2	5.5	500	0.48	79	95	76
	1100	1.5	5.5	500	0.48	85	95	82
	1100	1.9	5.5	500	0.48	88	95	85
KOH-F	900	1.2	3.5	500	0.48	69	98	66
	1100	1.2	3.5	500	0.48	83	95	80
	1300	1.2	3.5	500	0.48	87	91	84
KOH-G	900	1.2	13.5	500	0.48	68	98	65
	1100	1.2	13.5	500	0.48	75	95	72
	1300	1.2	13.5	500	0.48	78	91	75
				Kaolin + KCl				
KCl-A	1300	1.04	5.5	50	0.05	88	97	8
	1300	1.04	5.5	250	0.24	64	95	31

Table 4 continued

Exp. No.	T	τ	$Di_{Add.}$	K Conc.	$\frac{K}{Al+Si}$	$X_{K,\ exp}$	$X_{K,\ equi}$	$X_{(Al+Si)}$
	1300	1.19	5.5	500	0.48	50	52	48
	1300	1.04	5.5	750	0.72	35	36	50
	1300	1.04	5.5	1000	0.96	26	27	51
KCl-B	800	1.19	5.5	50	0.05	77	99	7
	900	1.19	5.5	50	0.05	80	99	8
	1300	1.04	5.5	50	0.05	81	97	8
	1450	1.04	5.5	50	0.05	81	94	8
KCl-C	800	1.19	5.5	500	0.48	31	81	29
	900	1.39	5.5	500	0.48	50	62	48
	1100	1.19	5.5	500	0.48	48	53	46
	1300 [j]	1.19	5.5	500	0.48	50	52	48
	1450	1.19	5.5	500	0.48	37	52	36
KCl-D	1100	0.81	5.5	500	0.48	42	53	41
	1100	1.19	5.5	500	0.48	48	53	46
	1100	1.6	5.5	500	0.48	50	53	48
	1100	1.87	5.5	500	0.48	49	53	47
KCl-E	1300	0.62	5.5	500	0.48	49	52	47
	1300	0.81	5.5	500	0.48	51	52	49
	1300	1.04	5.5	500	0.48	50	52	48
	1300	1.6	5.5	500	0.48	54	52	52
	1300	1.87	5.5	500	0.48	52	52	50
				Kaolin + K_2SO_4				
K_2SO_4-A	1100	1.2	5.5	50	0.05	68	100	7
	1100	1.2	5.5	500	0.48	43	100	41
	1100	1.2	5.5	1000	0.96	22	58	42
K_2SO_4-B	800	1.2	5.5	500	0.48	18	63	17
	900	1.2	5.5	500	0.48	37	63	36
	1100 [k]	1.2	5.5	500	0.48	43	100	41
	1300	1.2	5.5	500	0.48	38	100	37
	1450	1.2	5.5	500	0.48	27	84	26

[a] Residence time of gas and kaolin in hot zone of EFR.

[b] Mass-median-diameter of kaolin particles.

[c] Molar fraction of K atom in gas.

[d] Molar ratio of inlet elements.

[e] Potassium conversion from experimental measurements.

[f] Potassium conversion from equilibrium calculation. Note that Ω=$X_{K,\ equi}$/100.

[g] Estimated using present stoichiometric coefficient (Ψ).

[h] This line repeats data from KOH-A.

[i] This line repeats data from KOH-C.

[j] This line repeats data from KCl-A.

[k] This line repeats data from K_2SO_4-A.

* K_2CO_3 is injected into the reactor to form gaseous KOH.

Transport limitations

Figure 1 shows the temperature variation of binary diffusion coefficient of KOH (D_{KOH}) and KCl (D_{KCl}) in a nitrogen environment. The calculated effective diffusion coefficients (D_{eff}) of both KOH and KCl in the product-layer are also shown. All diffusion coefficients increase moderately as the function of temperature. The model for D_{eff} (equation 12) assumes that the gaseous alkali species diffuse in the pores of the product layer, and the porosity properties of the product-layer remains constant through conversion. In reality, phase change and pore closure likely take place and the alkali species may need to diffuse in a melted phase at high temperatures. The model has an reasonable agreement with the experimental conversion (see section), however the diffusion of potassium in the product layer is a relevant subject for future studies.

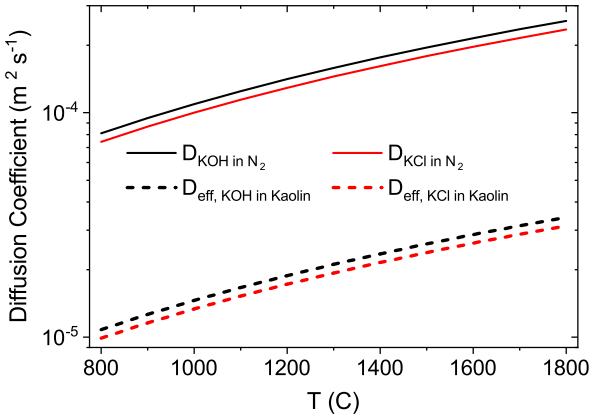

Figure 1: Binary diffusion coefficient ($D_{KOH\,in\,N_2}$ and $D_{KCl\,in\,N_2}$) and effective diffusion coefficient (D_{eff}) of KOH and KCl versus temperature.

Equilibrium calculation

An example of the products distribution at equilibrium for kaolin mixed with KOH is shown in Fig. 2. The inlet conditions are from experimental series of KOH-C (see Table 4), where kaolin, air, and KOH, along with trace amounts of water and ethanol, are injected into the reactor. Potassium is mainly captured as $KAlSiO_4$ at low temperatures, while it is mainly

captured as $KAlSi_2O_6$ or is released as KOH at higher temperatures. As a result, Ω gradually decreases until ~1500° C, and it stabilizes around 0.52 above 1500° C.

Figure 2 also presents products distribution at equilibrium for kaolin mixed with KCl. Here, switching from $KAlSiO_4$ to $KAlSi_2O_6$ is observed at 900° C, much lower than that in the KOH mixture. Above 950° C, $KAlSi_2O_6$ will be the major captured potassium components and KCl fraction drops gradually due to formation of Cl(g) and KOH. The value of Ω is around 0.53 after 950° C.

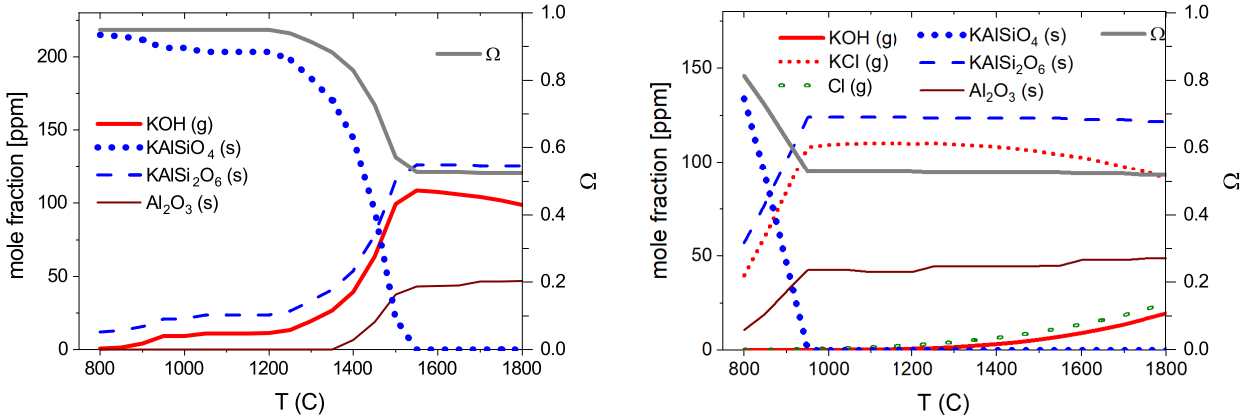

Figure 2: Equilibrium distribution of components accommodating major share of K/Al/Si/Cl. Left: Inlet conditions correspond to the series KOH-C (inlet: $N_{727812}\,O_{219288}\,H_{51155}\,C_{1018}\,Si_{252}\,K_{239}\,Al_{227}\,Fe_3\,Mg_2\,Na\,Cl\,Ca\,P$), Right: Inlet conditions correspond to the series KCl-C (inlet: $N_{715321}\,O_{220850}\,H_{61643}\,C_{1246}\,Si_{248}\,K_{235}\,Cl_{227}\,Al_{223}\,Fe_3\,Mg_2\,Na\,Ca\,P$). K/(Al+Si) is ~ 0.5 for both, see Table 4 for details.

Estimation of $k_{c,SCM}$ and $k_{c,UCM}$

Both modelling approaches require estimation of the rate coefficients (k_c) for the reaction between kaolin and potassium salts. Chemical kinetic supposedly controls the kaolin conversion at lower temperatures while diffusion and equilibrium constraints possibly dominate at higher temperatures[7,8]. In this work, the values of $k_{c,SCM}$ and $k_{c,UCM}$ are optimized to have the best available agreement between the model predictions and experimental data at low temperatures. The Arrhenius coefficients obtained this way are then used in the modelling

all experimental data from the EFR.

Table 4 lists $X_{K,\,equi}$, which is the equilibrium ceiling for potassium conversion in percentage, i.e., $X_{K,\,equi} = 100 \times \Omega$. The smaller equilibrium ceiling indicates stronger influence of equilibrium. The KOH-B series (800–1450° C, 50 ppm KOH, 5.5 μm) reported data from experiments with low salt concentration. Those data were prone to larger uncertainty due to difficulties in collecting and quantifying the low concentration of potassium components in the exhaust of the reactor[7]. Hence, the KOH-B series are neglected when fitting the Arrhenius rate coefficients.

Data of the KOH-G series (900–1300° C, 500 ppm KOH, 13.5 μm) cannot be reproduced by the SCM, even if either D_{eff} or $k_{c,SCM}$ increases within a reasonable range. The same level of conversion can be achieved only if both D_{eff} and $k_{c,SCM}$ increase simultaneously, which ruins the model prediction of other conditions. Similarly, the UCM approach needs much larger rate coefficient to reproduce the KOH-G points, so the KOH-G series are neglected when fitting the chemical kinetic rate coefficients.

Optimized rate coefficients at low temperatures (800–900° C) from series of KOH-C, KOH-C*, KOH-D, and KOH-F are less affected by equilibrium as confirmed by the large values of $X_{K,\,equi}$. Figure 3 shows the fitted rate coefficients and the low-temperature data. To have a better overall model prediction, the Arrhenius rate coefficients is fitted to KOH-C and KOH-D data, and can be represented by equations (14) and (15).

$$k_{c,SCM} = 12 \times e^{-5612/T} \tag{14}$$

$$k_{c,UCM} = 3.17 \times 10^4 \times e^{-5056/T} \tag{15}$$

Here, $k_{c,SCM}$ and $k_{c,UCM}$ are given in $(m\,s^{-1})$ and $(m^3\,mol^{-1}\,s^{-1})$, respectively. T represents temperature in Kelvin. The derived rate coefficients agree reasonably with KOH-C*, where K_2CO_3 was injected to produce in-situ gaseous KOH.

Fitting $k_{c,UCM}$ and $k_{c,SCM}$ for the kaolin reaction with KCl is more challenging as equilib-

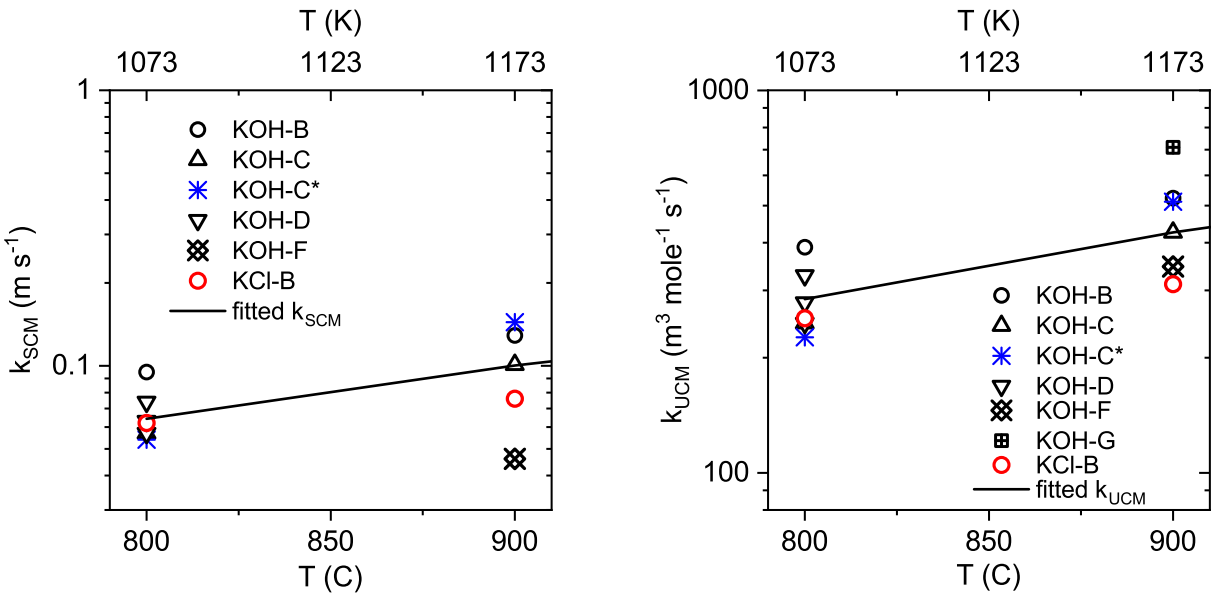

Figure 3: Selected chemical kinetic rate coefficients for the SCM (left) and the UCM (right) at low temperatures. Lines denote fitted Arrhenius rate coefficients. See text for further details.

rium emerges as the most important factor in capturing potassium, even at low temperatures. The KCl-C series is significantly affected by equilibrium limitations while the data from KCl-B have a larger uncertainty due to lower salt concentration, similar to KOH-B. Taking the larger uncertainties into account, the KCl-B series can be fairly well reproduced by using the rate coefficients fitted for kaolin + KOH (see Fig. 3), so the coefficients in equations (14) and (15) are also adopted for kaolin + KCl.

Modelling predictions

KOH capture by kaolin

Figure 4 shows examples of potassium conversion and additive consumption predicted by the present models. Figures 5 and 6 show the results of KOH conversion in reaction with kaolin. In the series KOH-A to KOH-E, the temperature changes from 800 to 1450° C, the gaseous potassium concentration changes from 50 to 1000 ppm (corresponding to a change in feed molar ratio of $\frac{K}{Al+Si}$ from 0.05 to 0.96), and the gas residence time changes from 1.2

to 1.9 s, while the size of fed kaolin particle is 5.5 μm. Both SCM and UCM follow closely the experimental results from KOH-A to KOH-E where KOH feed level, temperature, and residence time have been changed. The very minor differences between the results from direct injection of KOH and dissociation from K_2CO_3 indicates good repeatability of the experiments.

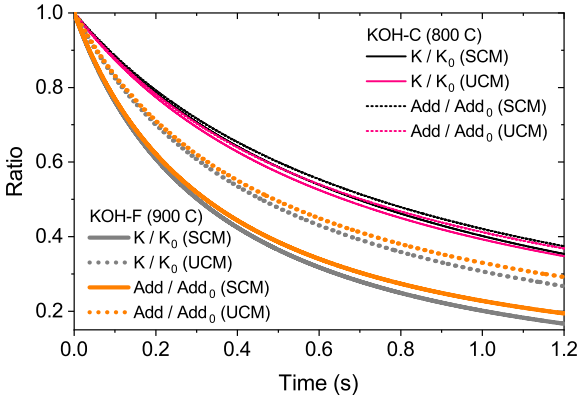

Figure 4: Evolution of potassium salt (K) and additive (Add) versus time. Data correspond to KOH-C at 800° C and KOH-F at 900° C. K_0 and Add_0 correspond to inlet values of the potassium salt and additive, respectily.

The KOH-F experiments (Fig. 6) were conducted with finer kaolin particles (3.5 μm). Here, the model predictions are less accurate, but still provide a reasonable agreement with the experimental data. The SCM model over-predicts the potassium capture slightly while the UCM is very close to the experimental points. The experiments of KOH-G were conducted with larger kaolin particles (13.5 μm). Here, the SCM under-predicts the conversion considerably while the UCM is closer to the experimental data. It seems that the SCM approach exaggerates the influence of particle size under present conditions.

The model performance can be further investigated via sensitivity analyse of potassium conversion to different parameters. The sensitivity coefficients (SEN) are calculated according to equation (16).

$$SEN = \frac{\Delta X_K / X_{K,0}}{\Delta Z / Z_0} \tag{16}$$

X_K is the potassium conversion and Z represents an independent parameter. Investigated

independent parameters are k_c, k_g, D_{eff}, and Ω, which represent effects of chemical kinetic, external diffusion, product-layer diffusion, and thermochemical equilibrium ceiling, respectively. The value of $\frac{\Delta Z}{Z_0}$ is selected as 20% to mimic a small change in the independent parameters.

Figure 7 shows the sensitivity of the model predictions for KOH capture with kaolin. The results confirm the dominance of the equilibrium in predicting the K-conversion at the higher temperatures. In most cases, the external diffusion plays a minor role, while chemical kinetic is the controlling mechanism at the lower temperatures. For the KOH-G series (900–1300° C, 500 ppm K_{gas}, 13.5 μm kaolin particle), the sensitivities of all parameters are comparable. To improve the SCM prediction for the KOH-G series at 900° C, increasing rate coefficient is needed. However, any increase in kinetic rate would cause over-prediction of potassium conversion in all series which are controlled by chemical kinetic.

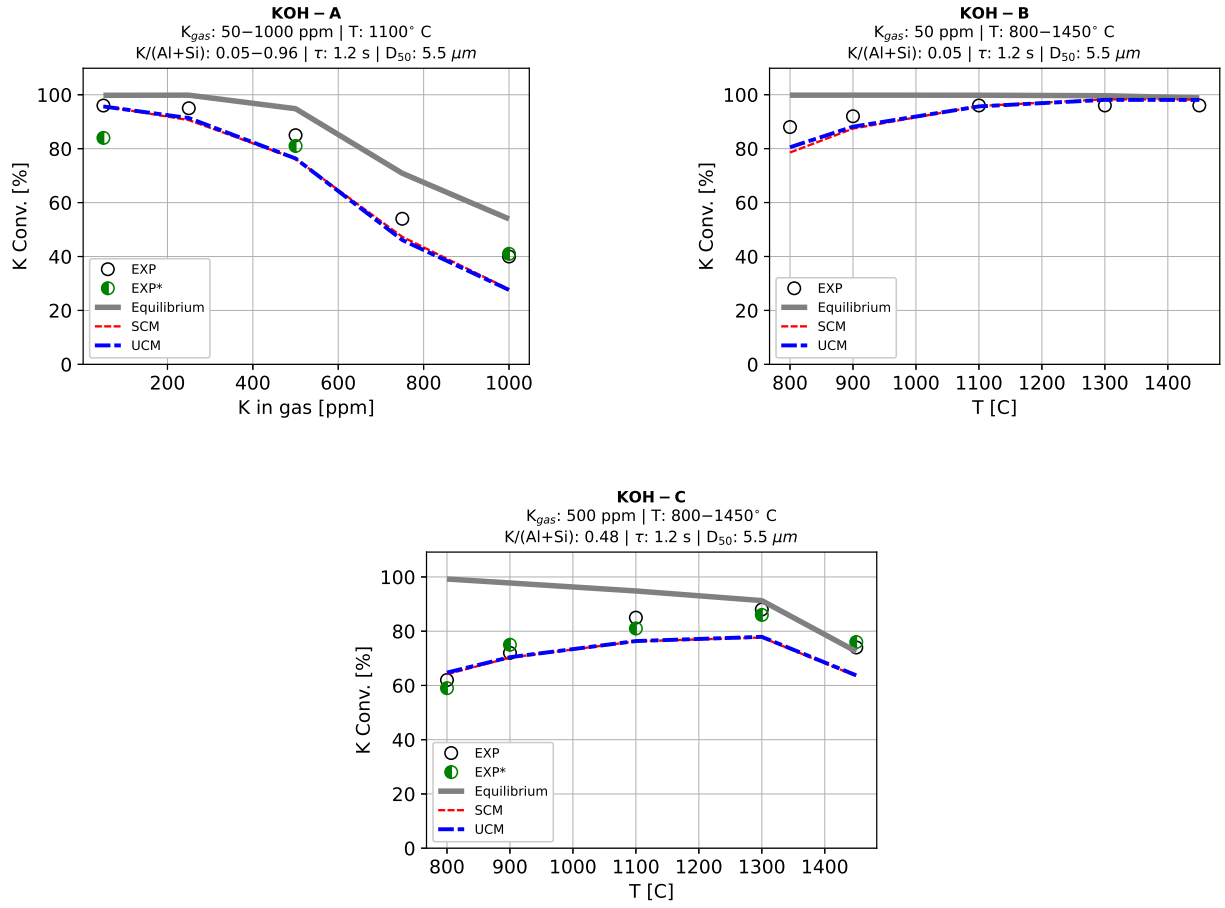

Figure 5: Potassium conversion for Kaolin + KOH. Experimental data from Wang et al.[7]. Consult figure title for detailed information. EXP* corresponds to the experiments using K_2CO_3 to produce in-situ gaseous KOH.

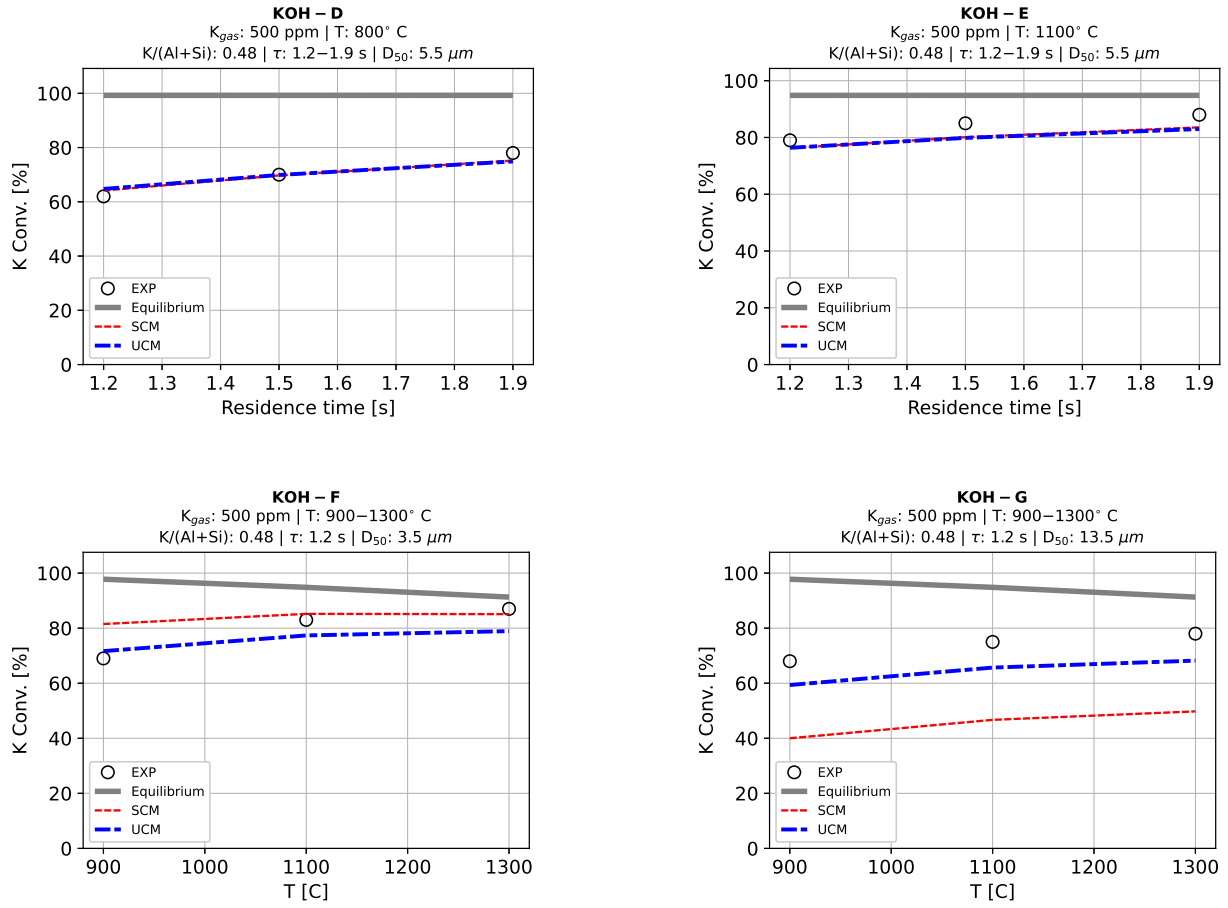

Figure 6: Potassium conversion for Kaolin + KOH. Experimental data from Wang et al.[7]. Consult figure title for detailed information.

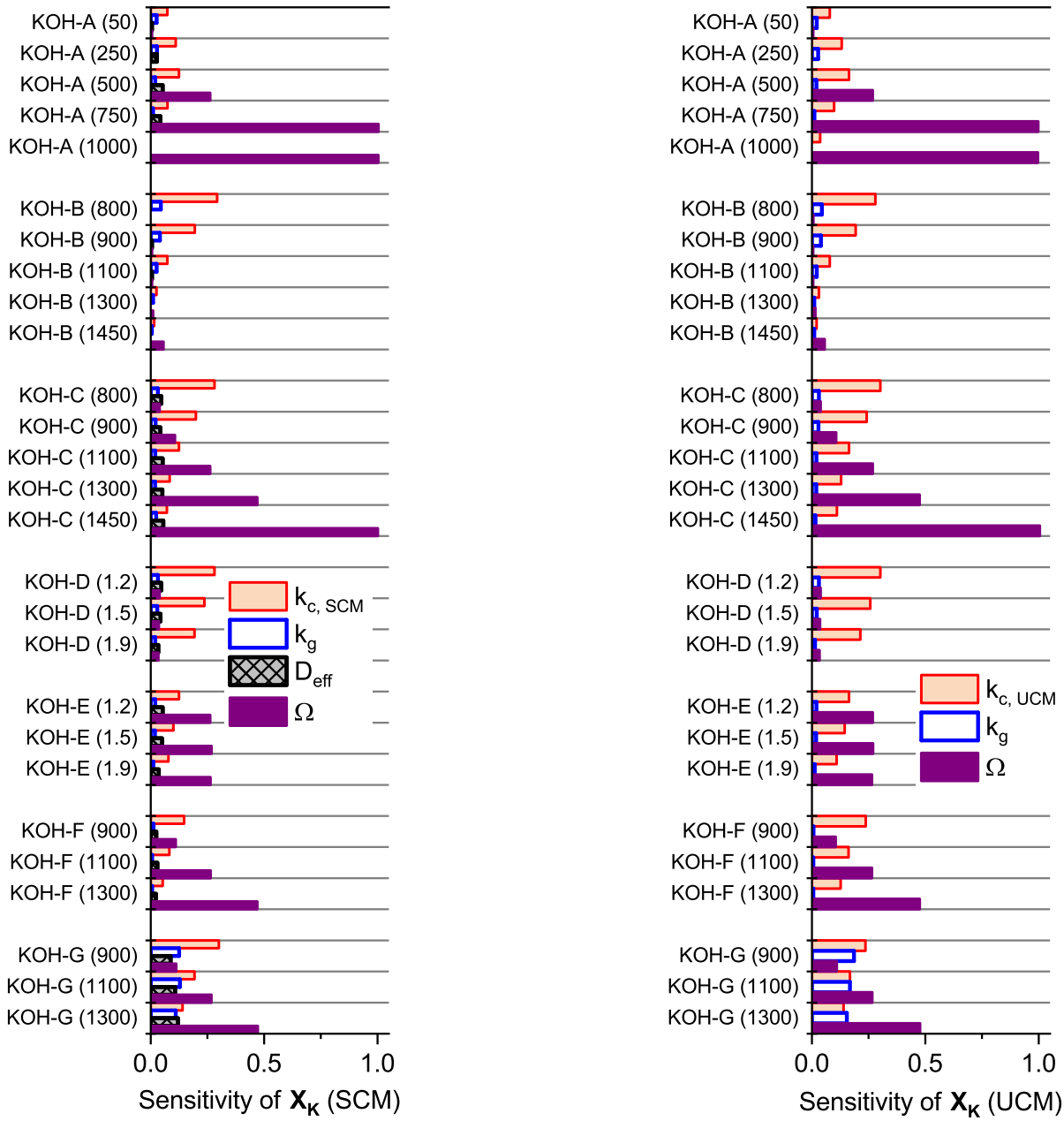

Figure 7: Sensitivity of K conversion for KOH + Kaolin. k_c, k_g, D_{eff}, Ω, and τ represent effects of chemical kinetic, external diffusion, product-layer diffusion, chemical equilibrium, and residence time, respectively.

KCl capture by kaolin

Figure 8 shows the results of KCl capture. The kinetic reaction rate coefficient is adopted from the KOH model. The predicted potassium conversion by the SCM and UCM models are very similar. The trends are well reproduced, but the predictions deviate from experimental data at some points. The potassium conversion is slightly over-predicted for low concentrations of potassium in series KCl-A and KCl-B, while the conversion is slightly under-predicted for other conditions.

Figure 9 presents the results of the sensitivity analysis for the KCl conversion predicted by the model. Chemical equilibrium controls potassium capture in most investigated series, and the sensitivity of chemical kinetic is comparable to the diffusion in the product layer (D_{eff}). The only exception is KCl-B (50 ppm of K_{gas}), where kinetic governs the conversion at 800–900° C.

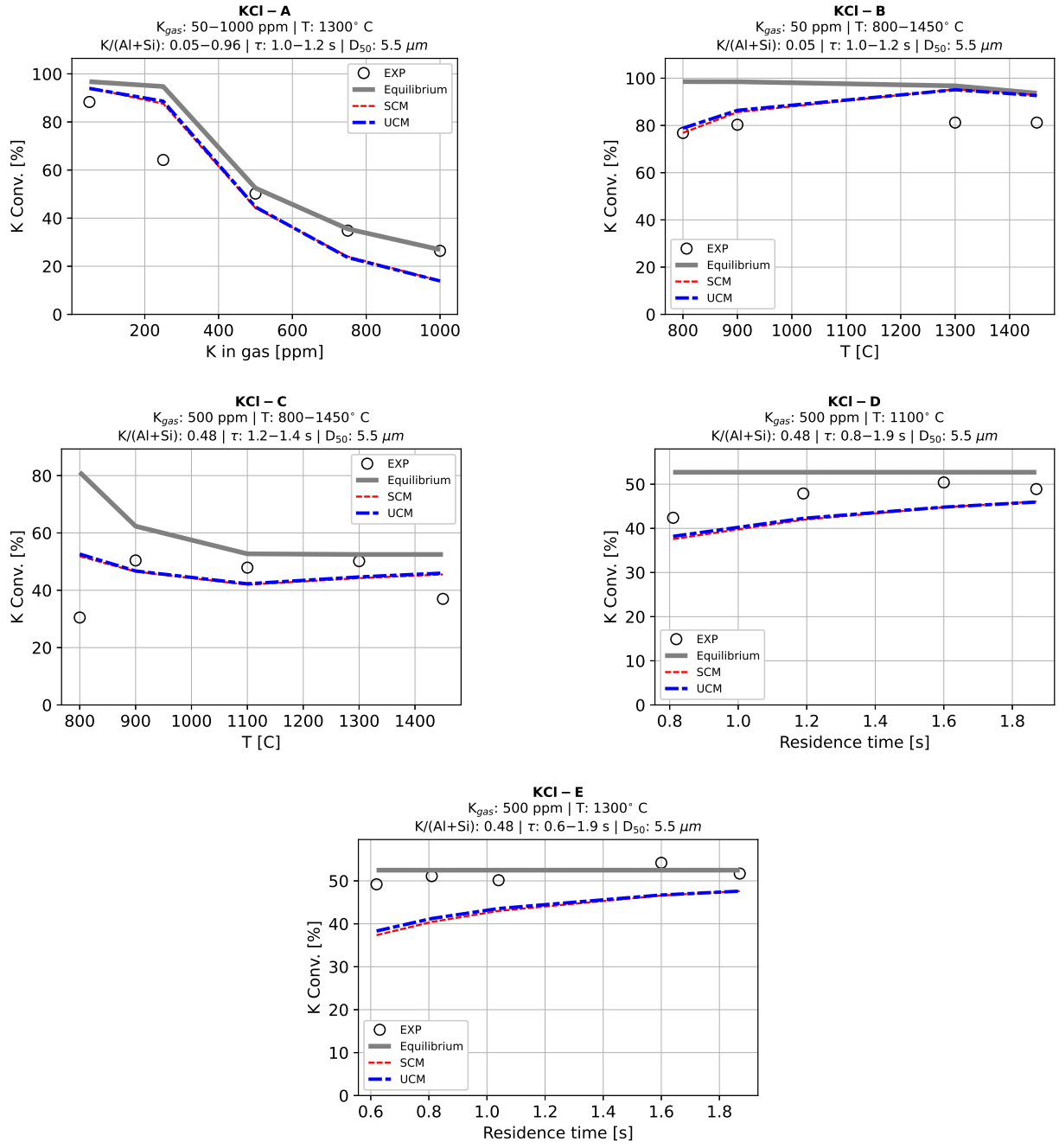

Figure 8: Potassium conversion for Kaolin + KCl. Experimental data from Wang et al.[8]. Consult figure title for detailed information.

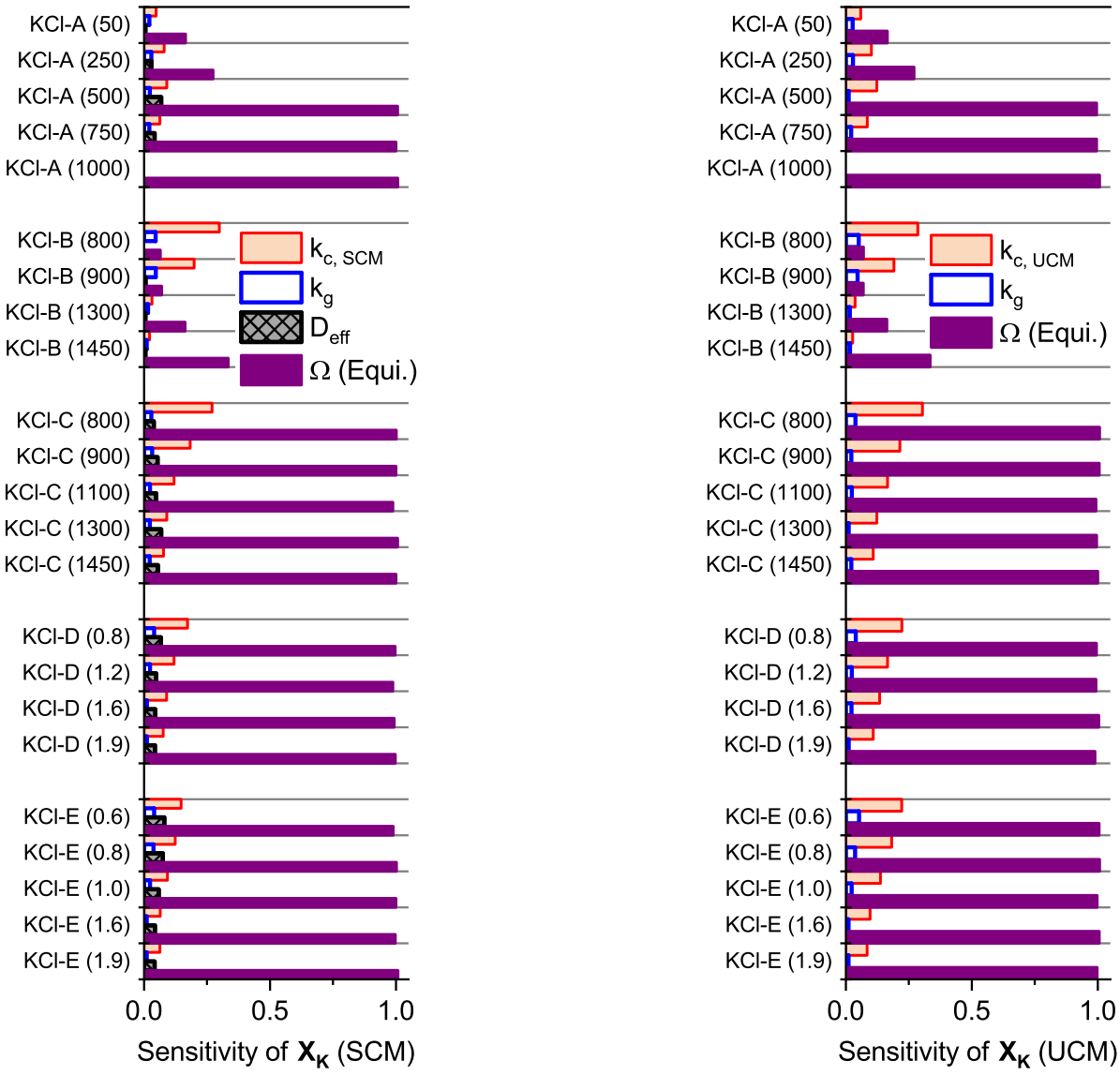

Figure 9: Sensitivity of K conversion predicted by models for KCl + Kaolin. k_c, k_g, D_{eff}, and Ω represent effects of chemical kinetic, external diffusion, product-layer diffusion, and chemical equilibrium, respectively.

K_2SO_4 capture by kaolin

As have been seen earlier for KOH and KCl capture with kaolin, the equilibrium model plays a critical role in predicting potassium conversion, especially at high temperatures. An example of product distribution at equilibrium stage for kaolin reaction with K_2SO_4 is shown in Fig. 10. Here, Ω peaks at intermediate temperature, a behaviour quite different from what has been observed for other salts (see Fig. 2). At the temperatures of 1000–1400° C, the equilibrium calculations predicted that potassium should be mainly captured as $KAlSiO_4$ (kalsilite), similar to the results from KOH calculation. However, the measurements in ref[8] indicated that $KAlSi_2O_6$ (leucite) is the major product for mixtures containing K_2SO_4, which means that less potassium can be bound in reality.

Due to large interference of equilibrium with data collected from K_2SO_4 experiments, extracting k_{SCM} and k_{UCM} is not possible, so the rate constants derived from KOH data is adopted here. If the present results from equilibrium calculation for K_2SO_4 reaction is adopted in the SCM and UCM models, both models predict a much higher conversion than the experiments for most cases (see Fig. 11). It is likely that the over-prediction problem is at least partially due to uncertainties in thermochemical equilibrium calculation for mixtures of kaolin and K_2SO_4.

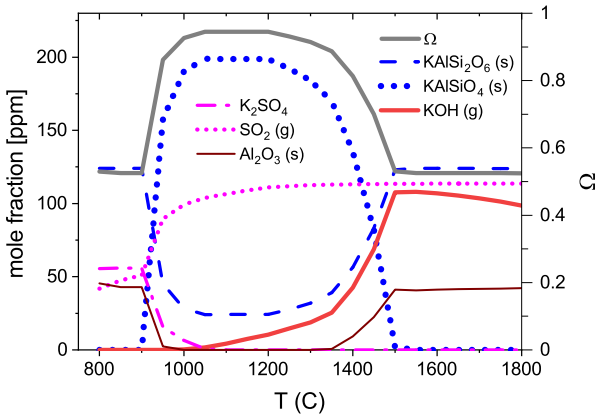

Figure 10: Equilibrium distribution of components accommodating major share of K/Al/Si for kaolin + K_2SO_4. Initial conditions correspond to K_2SO_4-A (X_K=500 ppm, K/(Al+Si)=0.5, inlet: $N_{716925}\,O_{220655}\,H_{60362}\,C_{1229}\,Si_{248}\,Al_{223}\,K_{236}\,S_{114}\,Fe_3\,Mg_2\,Ca\,P\,Na\,Cl$).

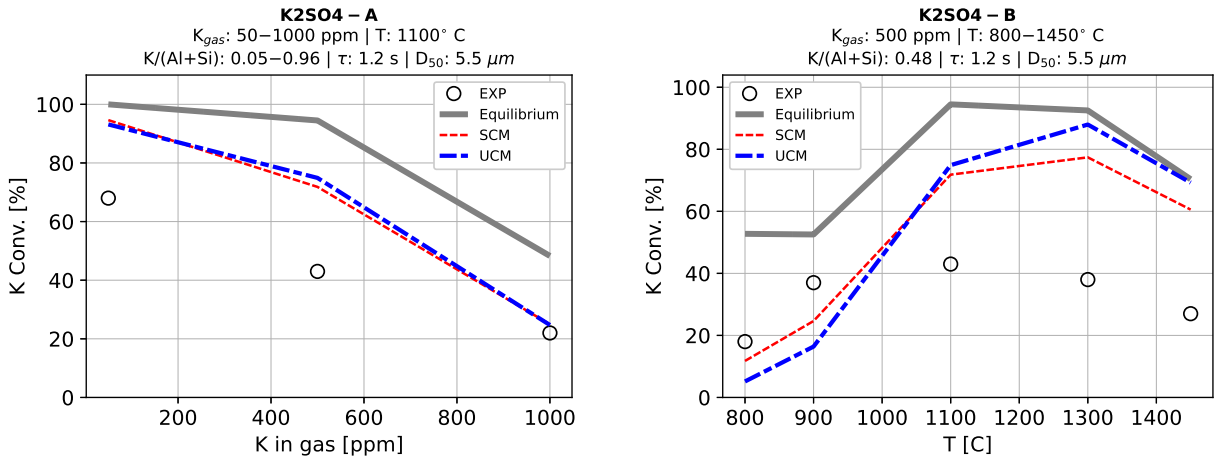

Figure 11: Potassium conversion for Kaolin + K_2SO_4. Experimental data from Wang et al.[8]. Consult figure title for detailed information.

Discussion

Figure 12 compares the predictions of both SCM and UCM models with the measured data. As demonstrated earlier, the predictions of both models are partially affected by the adopted chemical kinetic rate coefficients. Earlier suggestions for the chemical kinetic rate of potassium scavenging with kaolin are limited[12,13]. Tran et al.[12] suggested that the reaction rate follows $RR = k \times [KCl]^{1.5}$ where k is given as 1.44×10^{-4} ($m^3_{gas}\ m^{-3}_{solid}\ s^{-1}$) at 850° C. However, their rate coefficient is likely affected by the diffusion-resistance of salt into the product-layer, since large kaolin pellets (0.5–2 mm) were employed and exposed to KCl for a long time. A more complicated model was advocated by Zheng et al.[13] who took into account the gradient of gaseous potassium inside the large kaolin pellets in addition to the chemical kinetic restrictions. At 900° C, their fitted values for D_{eff} and k were 4.5×10^{-6} ($m^2\ s^{-1}$) and 3907 ($m^3_{gas}\ m^{-3}_{solid}\ s^{-1}$), respectively. Comparing the kinetic rate coefficients from the present work to those advocated in ref[13] is not straightforward due to fundamental differences in the modelling approaches. However, their estimated D_{eff} at 900° C ($4.5 \times 10^{-6}\ m^2\ s^{-1}$) is in the vicinity of the value advocated here ($1.3 \times 10^{-5}\ m^2\ s^{-1}$).

A more recent model by Zhu et al.[49] considered two reactions competing for additive as

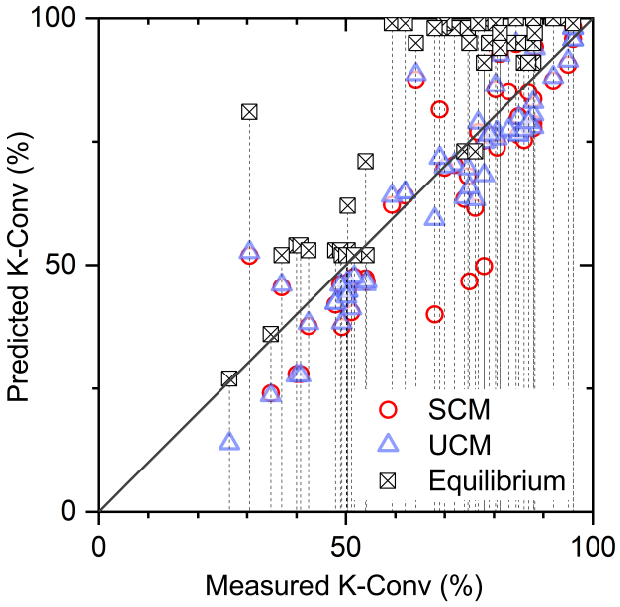

Figure 12: Comparison between the SCM and UCM predictions, equilibrium limits, and experimental data for all investigated conditions. The data for K_2SO_4 conversion are omitted.

R7a and R7b.

$$\text{Kaolin (s)} + \text{KOH (g)} \longrightarrow \text{Products (s)} \tag{R7a}$$

$$\text{Kaolin (s)} + \text{Products (s)} \longrightarrow \text{Products (s)} + \text{deactivated Kaolin (s)} \tag{R7b}$$

Zhu et al. have fitted the rate of both reactions to KOH data in Wang et al.[7], avoiding any direct input from thermochemical equilibrium. Generally speaking, the accuracy of the present model and that advocated by Zhu et al.[49] is close for most conditions. Predictions of both models have deviated from experimental data for large particles (13.5 μm, KOH-G). Another recent study by Chen et al.[50] used a similar approach to that in Zhu et al.[49] to account for additive deactivation. As demonstrated earlier, thermochemical equilibrium plays a critical role in potassium conversion at high temperatures, so the equilibrium ceiling should be calculated and imposed directly in modelling, especially if extrapolation to new conditions is desired. The model presented in this work relied on independent thermochemical equilibrium calculations, so its prediction might be more reliable for new conditions.

A complicated aspect in modelling additive reactivity has been the melting and transformation of additive particles which can affect mass transfer. The melting point of neat kaolinite is around 1750° C[63], but the formation of by-products might cause some melting, as found in ref[7]. According to Wang et al.[7], the reacted kaolin particles showed signs of melting even at temperature as low as 1300° C, likely due to the formation of some amorphous products. Wang et al.[64] investigated the calcination of kaolin in EFR and found that kaolin particles which melted at 1450° C had contained larger amounts of K, Na, Ca and Fe, so impurities in kaolin decreased the melting point considerably. Melting of doped kaolin particles has also been reported in sodium scavenging investigation[14,17]. Alongside melting, the transformation of the kaolin particle structure might affect kaolin reactivity[13,17].

The effect of additive melting on reaction progress is not monotonic[13]. Zheng et al.[13] suggested that kaolin phase transformation inhibits the potassium diffusion below 1300° C, while it has an opposite effect at higher temperatures. Gale and Wendt[17] suggested that kaolin phase transformation promotes the sodium conversion between 1130° C and 1230° C. However, as reported in ref[7,8] and confirmed here, chemical equilibrium likely controls the potassium conversion above 1300° C under the conditions of the present study. Since chemical equilibrium is independent of the initial structure and phase of reactants, melting and phase transformation should not have a considerable influence on the modelling results under conditions of the present work.

As shown earlier, the difference between the SCM and UCM models are negligible under most conditions, except when the size of particle increases to 13.5 μm. Both models include external diffusion resistance, which seems negligible for conditions investigated here. The product-layer assumed in the SCM model decelerates the diffusion of gas to the surface of the unreacted core. Punjak and Shadman[14] showed that in kaolin reaction with NaCl at 800° C, a product layer is formed around the kaolin flakes with the size of$\sim$7 mm. They also found that diffusion into the product-layer is much faster than the diffusion in interior of kaolin flakes. The present results also indicate that the diffusion resistance in the product-layer,

which has only been considered in the SCM model, has only had a minor effect on the kaolin conversion for particles of 6 μm and smaller. Consequently, the absence of the product-layer treatment in the UCM should not impose high uncertainties in the UCM predictions. However, apart from treatment of diffusion in the product-layer, SCM and UCM models are fundamentally different. In the SCM, the reaction only takes place on the outer surface of the unreacted core, and the alkali gas cannot penetrate inside the unreacted core. In the UCM model, the alkali gas can access the whole additive without any resistance.

In principle, it is less likely that the whole internal surface of large particles are equally exposed to the gaseous salts. Therefore less accuracy is expected for the UCM modelling of large particles. However, for very fine and porous kaolin particles as investigated here, the UCM seems to be more accurate. On the other hand, for porous materials same as kaolin, it is likely that the gas diffuse into the unreacted core, in contrast to the SCM assumptions. Therefore, a modified SCM model which allows partial diffusion of gas into the unreacted core might be of interest. All in all, both SCM and UCM are accurate enough for kaolin particles of 4–6 μm under the present conditions.

Conclusion

Two models (SCM and UCM) were developed for the reaction between solid kaolin and gaseous potassium compounds (KOH, KCl, and K_2SO_4) under pulverized-fuel (PF) boiler conditions. Both models accounted for conversion control by external mass transfer, kinetic, and equilibrium limitations, while the SCM also included the influence of diffusion in a product layer. Literature data for low-temperature (800–900° C) measurements in an entrained flow-reactor were used to derive chemical kinetic rate coefficients for the reaction between kaolin and KOH. The derived rate coefficient was then implemented in the models for the reaction between kaolin and all investigated potassium salts. The limitations of chemical equilibrium on potassium conversion was determined by using the *FactSage* database. Sen-

sitivity analyses indicated that chemical equilibrium controlled the potassium capture at the higher temperatures of the present study. There is a large deviation between equilibrium limit calculated for capturing K_2SO_4 by kaolin and the experimental results, which might be due to uncertainties in the chemical equilibrium calculation of mixtures containing sulphur. Both SCM and UCM could predict reasonably the conversion of potassium in reaction with kaolin particles of 4–6 μm. However, comparing to the experiments, it seems that the SCM exaggerated the influence of increasing the size of kaolin particles to 14 μm.

Further measurements of KCl reaction with kaolin at low temperatures and low $^{K}/_{(Al+Si)}$ molar ratio, where less equilibrium effect is expected, can be beneficial for extracting chemical kinetic rate coefficients dedicated to KCl. Investigating the porosity properties, phase transformation, and melting behaviour of kaolin and their effects on kaolin reactivity is suggested. This might lead to a better model of diffusion of alkali salt in the product-layer of kaolin particles. Experiments at higher temperatures (1450–1800° C), covering the upper temperature range of PF boilers, can also facilitate extended evaluation of the present models. The developed models can predict the reaction of gas phase alkali salts as KCl and KOH with kaolin with a reasonable accuracy at conditions as they appear in PF boilers using biomass

Acknowledgement

Funding from Ørsted A/S is gratefully acknowledged.

Supporting Information Available

The following files are available free of charge.

- Mathematical description of the models and detailed results from the equilibrium calculations.

- Molar distribution of the reactor inputs for all investigated conditions

Nomenclature

Symbols	Definition	Units
A	External surface area	(m^2)
D_z	Diffusion coefficient of component z	$(m^2\ s^{-1})$
$D_{z,0}$	Diffusion coefficient of component z at reference conditions (1 atm, 298 K)	$(m^2\ s^{-1})$
D_{eff}	Effective diffusion coefficient of gas into product layer	$(m^2\ s^{-1})$
D_{50}	Mass-median-diameter of kaolin particles	$(\mu\, m)$
$k_{c,SCM}$	Chemical kinetic rate coefficient in SCM	$(m\ s^{-1})$
$k_{c,UCM}$	Chemical kinetic rate coefficient in UCM	$(m^3\ mol^{-1}\ s^{-1})$
$k_{overall,SCM}$	Overall rate coefficient in SCM	$(m\ s^{-1})$
$k_{overall,UCM}$	Overall rate coefficient in UCM	$(m^3\ s^{-1})$
k_g	Mass transfer coefficient	$(m\ s^{-1})$
MW	Molar mass	$(kg\ mol^{-1})$
N_z	Mole of component z	(mol)
P	Pressure	(Pa)
r_i	Initial radius of particle	(m)
r_s	Radius of unreacted core in SCM	(m)
RR_{SCM}	Rate of reaction in SCM	$(mol\ s^{-1})$
RR_{UCM}	Rate of reaction in UCM	$(mol^2\ m^{-3}\ s^{-1})$
Re	Reynolds number	*dimensionless*
Sc	Schmidt number	*dimensionless*
SEN	Sensitivity coefficient	*dimensionless*
Sh	Sherwood number	*dimensionless*
T	Temperature	(K)
t	Time	(s)
X	Molar conversion	*dimensionless*
Z	Independent parameter in sensitivity analysis	*dimensionless*
[z]	Concentration of component z	$(mol\ m^{-3})$
$[z]_\infty$	Free-stream concentration of component z	$(mol\ m^{-3})$
β	Specific number of kaolin particle per volume of the gas	(m^{-3})
Γ	Tortuosity	*dimensionless*
ρ	Density	$(kg\ m^{-3})$
σ_c	Constriction factor	*dimensionless*
ϕ_p	Porosity	*dimensionless*
Ψ	Stoichiometric coefficient	*dimensionless*
Ω	Equilibrium ceiling, the ratio of captured to inlet potassium at equilibrium	*dimensionless*

τ	Reaction time	s

References

(1) Jiang, L.; Sheng, C. Correlation of sub-micrometer ash formation from pulverized biomass combustion with ash composition. *Energy Fuels* **2019**, *33*, 5893–5902.

(2) Xu, M.; Yue, A.; Sheng, C. Modeling K-Containing Vapors Transforming into Sub-micrometer Particles in Flue Gas of Pulverized Straw Combustion. *Energy Fuels* **2020**, *34*, 440–449.

(3) Hansen, L. A.; Nielsen, H. P.; Frandsen, F. J.; Dam-Johansen, K.; Hørlyck, S.; Karlsson, A. Influence of deposit formation on corrosion at a straw-fired boiler. *Fuel Process. Technol.* **2000**, *64*, 189–209.

(4) Zheng, Y.; Jensen, A. D.; Johnsson, J. E. Laboratory investigation of selective catalytic reduction catalysts: Deactivation by potassium compounds and catalyst regeneration. *Ind. Eng. Chem. Res.* **2004**, *43*, 941–947.

(5) Zheng, Y.; Jensen, A. D.; Johnsson, J. E. Deactivation of V_2O_5-WO_3-TiO_2 SCR catalyst at a biomass-fired combined heat and power plant. *Appl. Catal., B* **2005**, *60*, 253–264.

(6) Zheng, Y.; Jensen, A. D.; Johnsson, J. E.; Thøgersen, J. R. Deactivation of V_2O_5-WO_3-TiO_2 SCR catalyst at biomass fired power plants: Elucidation of mechanisms by lab-and pilot-scale experiments. *Appl. Catal., B* **2008**, *83*, 186–194.

(7) Wang, G.; Jensen, P. A.; Wu, H.; Frandsen, F. J.; Sander, B.; Glarborg, P. Potassium capture by kaolin, Part 1: KOH. *Energy Fuels* **2018**, *32*, 1851–1862.

(8) Wang, G.; Jensen, P. A.; Wu, H.; Frandsen, F. J.; Sander, B.; Glarborg, P. Potassium Capture by Kaolin, Part 2: K_2CO_3, KCl, and K_2SO_4. *Energy Fuels* **2018**, *32*, 3566–3578.

(9) Wang, G.; Jensen, P. A.; Wu, H.; Frandsen, F. J.; Laxminarayan, Y.; Sander, B.; Glarborg, P. KOH capture by coal fly ash. *Fuel* **2019**, *242*, 828–836.

(10) Wang, G.; Jensen, P. A.; Wu, H.; Frandsen, F. J.; Laxminarayan, Y.; Sander, B.; Glarborg, P. Potassium capture by coal fly ash: K_2CO_3, KCl and K_2SO_4. *Fuel Process. Technol.* **2019**, *194*, 106115.

(11) Tran, K.-Q.; Steenari, B.-M.; Iisa, K.; Lindqvist, O. Capture of potassium and cadmium by kaolin in oxidizing and reducing atmospheres. *Energy Fuels* **2004**, *18*, 1870–1876.

(12) Tran, K.-Q.; Iisa, K.; Steenari, B.-M.; Lindqvist, O. A kinetic study of gaseous alkali capture by kaolin in the fixed bed reactor equipped with an alkali detector. *Fuel* **2005**, *84*, 169–175.

(13) Zheng, Y.; Jensen, P. A.; Jensen, A. D. A kinetic study of gaseous potassium capture by coal minerals in a high temperature fixed-bed reactor. *Fuel* **2008**, *87*, 3304–3312.

(14) Punjak, W.; Shadman, F. Aluminosilicate sorbents for control of alkali vapors during coal combustion and gasification. *Energy Fuels* **1988**, *2*, 702–708.

(15) Punjak, W.; Uberoi, M.; Shadman, F. High-temperature adsorption of alkali vapors on solid sorbents. *AIChE Journal* **1989**, *35*, 1186–1194.

(16) Mwabe, P. O.; Wendt, J. O. Mechanisms governing trace sodium capture by kaolinite in a downflow combustor. *Symp. (Int.) Combust.* **1996**, *26*, 2447–2453.

(17) Gale, T. K.; Wendt, J. O. Mechanisms and models describing sodium and lead scavenging by a kaolinite aerosol at high temperatures. *Aerosol Sci. Technol.* **2003**, *37*, 865–876.

(18) Kerscher, F.; Stetka, M.; Spliethoff, H. The Reaction Kinetics of Gaseous Alkali Capture by Kaolin in Syngas Atmosphere. *Chem. Eng. Technol.* **2018**, *41*, 1881–1888.

(19) Batir, O.; Selçuk, N.; Kulah, G. Effect of kaolin addition on alkali capture capability during combustion of olive residue. *Combust. Sci. Technol.* **2019**, *191*, 43–53.

(20) Schürmann, H.; Unterberger, S.; Hein, K.; Monkhouse, P.; Gottwald, U. The influence of fuel additives on the behaviour of gaseous alkali-metal compounds during pulverised coal combustion. *Faraday Discuss.* **2002**, *119*, 433–444.

(21) Shadman, F.; Punjak, W. Thermochemistry of alkali interactions with refractory adsorbents. *Thermochim. Acta* **1988**, *131*, 141–152.

(22) Uberoi, M.; Punjak, W.; Shadman, F. The kinetics and mechanism of alkali removal from flue gases by solid sorbents. *Prog. Energy Combust. Sci.* **1990**, *16*, 205–211.

(23) Li, Y.; Li, J.; Jin, Y.; Wu, Y.; Gao, J. Study on alkali-metal vapor removal for high-temperature cleaning of coal gas. *Energy Fuels* **2005**, *19*, 1606–1610.

(24) Takuwa, T.; Naruse, I. Detailed kinetic and control of alkali metal compounds during coal combustion. *Fuel Process. Technol.* **2007**, *88*, 1029–1034.

(25) Takuwa, T.; Naruse, I. Emission control of sodium compounds and their formation mechanisms during coal combustion. *Proc. Combust. Inst.* **2007**, *31*, 2863–2870.

(26) Xu, L.; Liu, J.; Kang, Y.; Miao, Y.; Ren, W.; Wang, T. Safely burning high alkali coal with kaolin additive in a pulverized fuel boiler. *Energy Fuels* **2014**, *28*, 5640–5648.

(27) Zhang, X.; Liu, H.; Xing, H.; Li, H.; Hu, H.; Li, A.; Yao, H. Improved sodium adsorption by modified kaolinite at high temperature using intercalation-exfoliation method. *Fuel* **2017**, *191*, 198–203.

(28) He, Y.; Whiddon, R.; Wang, Z.; Liu, Y.; Zhu, Y.; Liu, J.; Cen, K. Inhibition of sodium release from Zhundong coal via the addition of mineral additives: Online combustion

measurement with laser-induced breakdown spectroscopy (LIBS). *Energy Fuels* **2017**, *31*, 1082–1090.

(29) Steenari, B.-M.; Lindqvist, O. High-temperature reactions of straw ash and the anti-sintering additives kaolin and dolomite. *Biomass Bioenergy* **1998**, *14*, 67–76.

(30) Turn, S. Q.; Kinoshita, C. M.; Ishimura, D. M.; Hiraki, T. T.; Zhou, J.; Masutani, S. M. An experimental investigation of alkali removal from biomass producer gas using a fixed bed of solid sorbent. *Ind. Eng. Chem. Res.* **2001**, *40*, 1960–1967.

(31) Yang, H.-C.; Yun, J.-S.; Kang, M.-J.; Kim, J.-H.; Kang, Y. Mechanisms and kinetics of cadmium and lead capture by calcined kaolin at high temperatures. *Korean J Chem Eng* **2001**, *18*, 499–505.

(32) Wei, X.; Lopez, C.; von Puttkamer, T.; Schnell, U.; Unterberger, S.; Hein, K. R. Assessment of chlorine- alkali- mineral interactions during co-combustion of coal and straw. *Energy Fuels* **2002**, *16*, 1095–1108.

(33) Tran, K.-Q.; Iisa, K.; Hagström, M.; Steenari, B.-M.; Lindqvist, O.; Pettersson, J. B. On the application of surface ionization detector for the study of alkali capture by kaolin in a fixed bed reactor. *Fuel* **2004**, *83*, 807–812.

(34) Davidsson, K.; Steenari, B.-M.; Eskilsson, D. Kaolin addition during biomass combustion in a 35 MW circulating fluidized-bed boiler. *Energy Fuels* **2007**, *21*, 1959–1966.

(35) Escobar, I.; Müller, M. Alkali removal at about 1400° C for the pressurized pulverized coal combustion combined cycle. 2. Sorbents and sorption mechanisms. *Energy Fuels* **2007**, *21*, 735–743.

(36) Steenari, B.-M.; Fedje, K. K. Addition of kaolin as potassium sorbent in the combustion of wood fuel–Effects on fly ash properties. *Fuel* **2010**, *89*, 2026–2032.

(37) Bläsing, M.; Müller, M. Investigation of the effect of alkali metal sorbents on the release and capture of trace elements during combustion of straw. *Combust. Flame* **2013**, *160*, 3015–3020.

(38) Damoe, A. J.; Wu, H.; Frandsen, F. J.; Glarborg, P.; Sander, B. Impact of coal fly ash addition on combustion aerosols ($PM_{2.5}$) from full-scale suspension-firing of pulverized wood. *Energy Fuels* **2014**, *28*, 3217–3223.

(39) Xu, Y.; Liu, X.; Zhang, Y.; Sun, W.; Hu, Y.; Xu, M. A novel Ti-based sorbent for reducing ultrafine particulate matter formation during coal combustion. *Fuel* **2017**, *193*, 72–80.

(40) Chen, D.; Liu, X.; Wang, C.; Xu, Y.; Sun, W.; Cui, J.; Zhang, Y.; Xu, M. Effects of H_2O and HCl on particulate matter reduction by kaolin under oxy-coal combustion. *Energy Fuels* **2017**, *31*, 6455–6462.

(41) Liu, Y.; Duan, X.; Cao, X.; Che, D.; Liu, K. Experimental study on adsorption of potassium vapor in flue gas by coal ash. *Powder Technol.* **2017**, *318*, 170–176.

(42) Sun, W.; Liu, X.; Xu, Y.; Zhang, Y.; Chen, D.; Chen, Z.; Xu, M. Effects of the modified kaolin sorbents on the reduction of ultrafine particulate matter ($PM_{0.2}$) emissions during pulverized coal combustion. *Fuel* **2018**, *215*, 153–160.

(43) Fuller, A.; Omidiji, Y.; Viefhaus, T.; Maier, J.; Scheffknecht, G. The impact of an additive on fly ash formation/transformation from wood dust combustion in a lab-scale pulverized fuel reactor. *Renewable energy* **2019**, *136*, 732–745.

(44) Gehrig, M.; Wöhler, M.; Pelz, S.; Steinbrink, J.; Thorwarth, H. Kaolin as additive in wood pellet combustion with several mixtures of spruce and short-rotation-coppice willow and its influence on emissions and ashes. *Fuel* **2019**, *235*, 610–616.

(45) Zhang, X.; Liu, H.; Xing, H.; Wang, G.; Deng, H.; Hu, H.; Li, X.; Yao, H. Correlations between the sodium adsorption capacity and the thermal behavior of modified kaolinite during the combustion of Zhundong coal. *Fuel* **2019**, *237*, 170–177.

(46) Rebbling, A.; Fagerström, J.; Steinvall, E.; Carlborg, M.; Öhman, M.; Boman, C. Reduction of alkali release by two fuel additives at different bed temperatures during grate combustion of woody biomass. *Energy Fuels* **2019**, *33*, 11041–11048.

(47) Wu, H.; Glarborg, P.; Frandsen, F. J.; Dam-Johansen, K.; Jensen, P. A. Dust-firing of straw and additives: ash chemistry and deposition behavior. *Energy Fuels* **2011**, *25*, 2862–2873.

(48) Wu, H.; Bashir, M. S.; Jensen, P. A.; Sander, B.; Glarborg, P. Impact of coal fly ash addition on ash transformation and deposition in a full-scale wood suspension-firing boiler. *Fuel* **2013**, *113*, 632–643.

(49) Zhu, C.; Zhang, H.; Sheng, C. Modeling the Capture of KOH Vapor with Kaolin under Conditions of Pulverized Fuel-Fired Boilers. *Energy Fuels* **2021**, *35*, 7050–7057.

(50) Chen, S.; Cheng, M.; Xu, J.; Liu, X.; Yu, D.; Xu, M. Numerical Analysis on Reduction of Ultrafine Particulate Matter by a Kaolin Additive during Pulverized Coal Combustion. *Energy Fuels* **2021**, *35*, 9538–9549.

(51) Xing, H.; Liu, H.; Zhang, X.; Huang, B.; Huang, Y.; Hu, H.; Yao, H. Correlations between vapor-phase Na/K/As adsorption capacities of kaolinite and temperature-dependent derivation of its Al-containing groups. *Proc Combust Inst* **2021**, *38*, 5237–5247.

(52) Levenspiel, O. *The Chemical Reactor Omnibook*; Oregon State University Bookstores, 1993; Chapter 55.

(53) Reid, R.; Prausnitz, J.; Poling, B. *The Properties of Gases and Liquids*, 4th ed.; McGraw-Hill, 1987.

(54) Svehla, R. A. *Estimated viscosities and thermal conductivities of gases at high temperatures*; National Aeronautics and Space Administration, 1963; Vol. 132.

(55) Reaction Design, CHEMKIN Input Manual. 2013.

(56) Scott Fogler, H. *Elements of Chemical Reaction Engineering, 4th Ed.*; Pearson Education Limited, 2006; pp 813–816.

(57) Zheng, Y.; Jensen, P. A.; Jensen, A. Potassium Capture by Coal Minerals in a High Temperature Fixed Bed Reactor. 2007; MSc Thesis, Technical University of Denmark (DTU).

(58) Chen, C.; Lan, G.; Tuan, W. Microstructural evolution of mullite during the sintering of kaolin powder compacts. *Ceram. Int.* **2000**, *26*, 715–720.

(59) Niu, Y.; Tan, H.; Hui, S. Ash-related issues during biomass combustion: Alkali-induced slagging, silicate melt-induced slagging (ash fusion), agglomeration, corrosion, ash utilization, and related countermeasures. *Prog. Energy Combust. Sci.* **2016**, *52*, 1–61.

(60) Bale, C. et al. FactSage thermochemical software and databases, 2010–2016. *Calphad* **2016**, *54*, 35–53.

(61) Ansys Chemkin-Pro Release 2020 R1. 2020.

(62) Mortensen, M. R.; Hashemi, H.; Wu, H.; Glarborg, P. Modeling post-flame sulfation of KCl and KOH in bio-dust combustion with full and simplified mechanisms. *Fuel* **2019**, *258*, 116147.

(63) Varga, G. The structure of kaolinite and metakaolinite. *Epitoanyag* **2007**, *59*, 6–9.

(64) Wang, G. Potassium Capture by Kaolin and Coal Fly Ash. Ph.D. thesis, Technical University of Denmark (DTU), 2018.

TOC Graphic

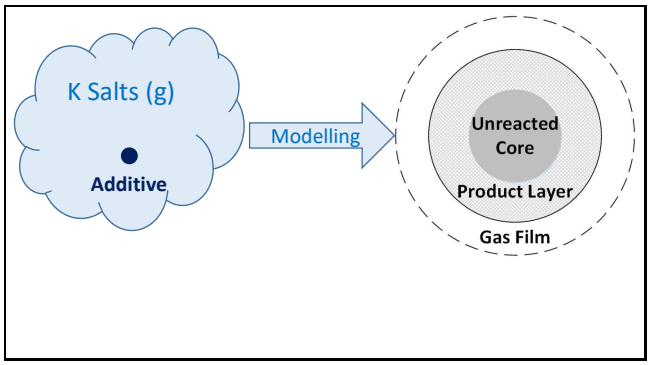
K Salts (g)
Additive
Modelling
Unreacted
Core
Product Layer
Gas Film